Research paper

Accuracy analysis in determining the location of underground objects using GPR involving lidar data

Anna Lejzerowicz[1], Paweł Czernic[2], Magdalena Pilarska-Mazurek[3], Kamil Załęgowski[4], Jakub Górka[5], Krzysztof Bakuła[6]

Abstract: Ground penetrating radar (GPR) is one of the most useful non-destructive techniques for locating underground objects. Advancements in this technology have facilitated the development of new sensors over the past decade. In this paper, an accuracy assessment of the location of underground objects using various GPR antennas is presented. To achieve the stated goals, measurements of 5 concrete slabs, reinforced with steel bars of various diameters and located at variable depths were taken. The experiment includes the usage of three GPR antennas to assess the format, characteristics, and differences of extracted data. This set of antennas from different manufacturers varied in terms of operating frequency. Additional lidar data from TLS (terrestrial laser scanning) was utilized in the methodology to provide precise surface measurements and therefore, external orientation of the surveyed data. The experiment allowed for the determination of vertical and horizontal accuracy for three tested antennas and the assessment of increasing errors value with greater depth of the measured items, which is important for surveying accuracy forecasting.

Keywords: concrete slab, GPR, lidar, reinforcement, TLS, visualization

---

[1]PhD., Warsaw University of Technology, Faculty of Civil Engineering, Al. Armii Ludowej 16, 00-637 Warsaw, Poland, e-mail: anna.lejzerowicz@pw.edu.pl, ORCID: 0000-0002-1350-0632

[2]Eng., Warsaw University of Technology, Faculty of Geodesy and Cartography, Pl. Politechniki 1, 00-661, Warsaw, Poland, e-mail: pawel.czernic.stud@pw.edu.pl, ORCID: 0009-0008-6927-5375

[3]PhD., Eng., Warsaw University of Technology, Faculty of Geodesy and Cartography, Pl. Politechniki 1, 00-661, Warsaw, Poland, e-mail: magdalena.pilarska@pw.edu.pl, ORCID: 0000-0001-9494-9863

[4]PhD., Eng., Warsaw University of Technology, Faculty of Civil Engineering, Al. Armii Ludowej 16, 00-637 Warsaw, Poland, e-mail: kamil.zalegowski@pw.edu.pl, ORCID: 0000-0002-9520-0288

[5]DSc., Eng., Warsaw University of Technology, Faculty of Geodesy and Cartography, Pl. Politechniki 1, 00-661, Warsaw, Poland, e-mail: jakub.gorka@pw.edu.pl, ORCID: 0000-0002-8262-847X

[6]PhD., Eng., Warsaw University of Technology, Faculty of Geodesy and Cartography, Pl. Politechniki 1, 00-661, Warsaw, Poland, e-mail: krzysztof.bakula@pw.edu.pl, ORCID: 0000-0001-7137-1667

1. Introduction

Ground penetrating radar (GPR) technology is commonly used in many applications concerning the location of underground objects because of its high resolution, high efficiency, and non-destructive characteristics [1]. GPR has found applications e.g. in archaeology [2], transport infrastructure [3] including concrete pavements [4], and in the monitoring of engineering structures [5]. One of the most popular GPR applications is pipe detection because their location is crucial for excavation works [6]. Accurate detection of the object location depends on the user's indication of the vertex of the diffraction hyperbola and velocity approximation of the wave in the investigated medium. Therefore, in many applications, the detection of the objects on radar-grams is conducted automatically and can eliminate the need for an operator [7].

A crucial feature of the GPR technology is antenna frequency. The lower the frequency, the deeper-located objects can be detected. On the other hand, the higher the frequency, the smaller the objects may be and still be found with precision. Thus, it is important to choose a suitable antenna for the selected purpose. Antennas of similar frequency can also provide different results owing to different sensor quality and technology used.

This paper describes the research on the innovative use of GPR technology that enables continuous and non-destructive surveying of the underground objects' positions. In this article, three different antennas were used for rebar detection in concrete slabs. The results derived from those antennas were compared and analyzed concerning similar research from the literature. The aim of the research was also to develop a GPR usage method with the inclusion of lidar (Light Detection and Ranging). The integration of lidar data was used to reinforce the completeness, credibility, and accuracy of the internal structure of the tested object. In the literature, the concept of GPR and lidar integration can already be found. The easiest way of data integration is using georeferenced GPR and georeferenced lidar data for further analysis, e.g. in archaeology [8]. In [9] lidar sensor was used for platform orientation. Lidar and GPR data can also be integrated for real-time data fusion [10]. In [4] the visual inspection of profiles derived from digital elevation models from airborne laser scanning (ALS) and GPR data was performed for archaeological structures analysis.

2. Materials and methods

This section briefly presents the basis of two technologies used together in the experiment to assess the quality of depth measurement of underground objects using the GPR method. In this section, their short description can be found.

2.1. Ground penetrating radar (GPR)

The ground penetrating radar method is a non-destructive, high-resolution electromagnetic method, perfectly suited for testing shallow sediments or road infrastructure. Due to its non-invasive nature, the GPR method can be used in places where invasive tests may, for

example, affect the structure of the tested object. There are many applications of the GPR method, e.g. inventory of underground infrastructure, arrangement of reinforcement, and control of the condition of road surfaces.

For GPR surveys, antennas with different ranges and measurement accuracy are used. The GPR method uses electromagnetic waves with frequencies usually in the range of 10–4000 MHz, while antennas with higher frequencies (in the range of several GHz) are used in engineering research. High-frequency antennas are characterized by a small depth range but high resolution of the acquired data. Antennas using lower frequencies have a higher depth range, but the resolution of radargrams is lower.

In GPR investigations, an electromagnetic wave (EM) pulse with a known, present frequency is sent by a transmitting antenna. The energy of the electromagnetic wave penetrating the medium at the boundaries of sediments or structural layers, with different electrical properties, is partially reflected and refracted [11, 12] as well as partially attenuated [13]. When returning, the reflected pulse is registered on the surface by the receiving antenna. The amplitude of the reflected electromagnetic wave is proportional to the magnitude of the reflection coefficient at the boundary of two different media (Fig. 1). On the recorded images (radargrams), we can see electromagnetic waves reflected from the boundaries of the media, which differ primarily in the values of the dielectric constant (ε_r). In simple terms, it can be stated that the quality of the data on the radargram, i.e. the strength of the reflections and the magnitude of the amplitude, depends on the contrast of the electrical properties between the two media.
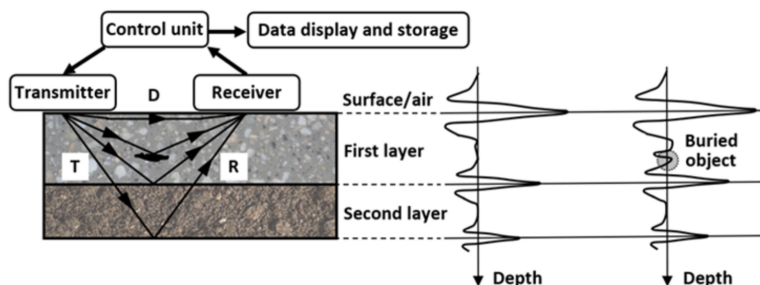

Fig. 1. The principle of operation of the GPR and the effect of a buried object on the radar signal reflection (T – transmitted impulse, R – reflected energy, D – direct arrival)

The basis of GPR operation is the emission of an electromagnetic wave and sending it to the concrete in this case. When it reaches the surface of the rebar embedded in the concrete, the EM wave is reflected and recorded by the ground penetrating radar. GPR can obtain the spatial characteristics of rebar by recording the two-way travel time of the EM wave. Typically, the hyperbola pattern is a form of presentation of the reflection of rebars in GPR data [14–16]. A hyperbola is created by the additional reflections produced by the rebar as the GPR passes over it [16]. When the GPR antenna moves directly over the rebar, the recorded travel time becomes the fastest at that location. On the other hand, the travel time increases as the GPR antenna moves away from the rebar [17]. The resulting graph of travel times is a hyperbola whose vertex indicates the exact position of the rebar (Fig. 2). Hyperbola

is a combination of rebar size, depth, the EM velocity in the concrete, scanning direction (if it's perpendicular to the rebar), and two-way travel time of the EM wave [18]. Even though the location of the rebar using GPR is already a mature technique [14–16, 19–22], it remains a challenge to precisely determine the cover thickness as well as the size of the rebar [23–25].
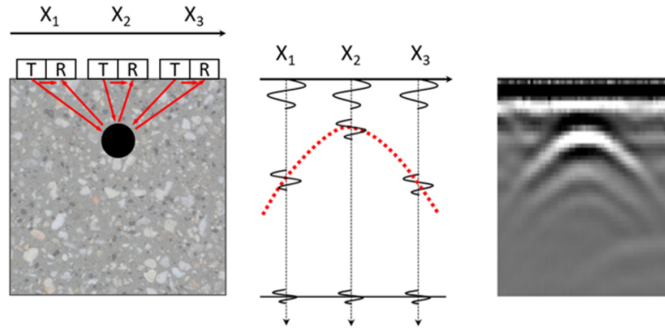

Fig. 2. Location of rebar in concrete: formation of a hyperbola in the radargram (T – transmitting antenna; R – receiving antenna; X_1, X_2, and X_3 – position of the GPR); the arrows show the direction of the antenna's movement on the ground above the searched object

2.2. Light detection and ranging (lidar)

Lidar is an active, non-invasive measurement method which consists of sending a beam from the laser to the object with very high frequency (thousands of points per second). After the beam reflects from the object, it returns to the scanner and the time of the beam route is determined. Based on the calculated scanner-object distance and the known angle at which the laser beam was sent, 3D information about the object is obtained. As a result, a point cloud that consists of thousands of measurements is provided. For every point in the cloud X, Y, and Z coordinates are assigned.

Lidar technology, like GPR, is a non-invasive, remote sensing method of measurement, and because of that, it has found application in many branches, such as engineering [26], geology [27], archaeology [28], and forestry [29]. The laser beam operates mostly in near infrared wavelengths (most popular are: 1064 nm and 1550 nm), sometimes in the green part of the spectrum (532 nm), which is safe for humans. Lidar data can be acquired from laser scanners mounted on cars (i.e. mobile laser scanning), unmanned aerial vehicles (UAVs) and airplanes (i.e. airborne laser scanning). Furthermore, lidar data can be acquired from stationary terrestrial laser scanners (TLS). As a result, for almost every kind of application, there is a possibility to find an optimal way to obtain lidar data.

In TLS, based on the distance from the scanner to the object and two angles: horizontal (azimuth) and vertical (elevation), 3D information about the object is obtained. Referring to [30], TLS presents a few advantages; first of all, a point cloud from TLS is characterized by very high density (hundreds/thousands of measurements per square meter) and can be captured relatively fast. Additionally, TLS measurement, as well as further data processing, is fully

automated. Furthermore, apart from geometric information, TLS data can deliver additional information, such as RGB colours and the intensity of the reflected laser beam. Moreover, terrestrial laser scanners can provide data with relatively high, millimeter or centimeter accuracy. Due to the penetration capability of the laser more than one return can be registered for a single beam, what is an advantage especially in vegetation analysis. It is suitable for many engineering applications, and in some research works, TLS data can be used as more accurate reference data. Crucially, TLS data can be delivered in a local coordinate system defined by the scanning system or in a global reference system determined by control points.

In this article, TLS data is used for georeferencing the GPR data and for performing a more detailed analysis of the concrete slabs. Within the article, the authors want to present the advantages of such a surveying method in this application.

3. Methodology

This section presents a description of the test site and the methodology of the experiment, including subsequent stages of research and a description of the obtained data with the employed antennas.

3.1. Test site description

To achieve the research objective, test measurements were carried out at the Testing Site for Nondestructive Methods of the Warsaw University of Technology. The entire testing site consists of fourteen slabs of $120 \times 80 \times 20$ cm which have artificially introduced discontinuities, while the fifteenth slab has no discontinuities and is treated as a reference. The controlled discontinuities of the investigated slabs are listed in Table 1 and presented in diagrams in Fig. 3.

Table 1. Controlled discontinuities of slabs

Slab no	Discontinuities	Dimensions of discontinuities	Depth of discontinuities
1	reinforcement (grid: 15×15 cm)	upper Ø 8 lower Ø 12	3 cm
2			5 cm
3		upper Ø 16 lower Ø 12	3 cm
4			5 cm
5	diversified cover of the reinforcement	Ø 12	from 2.5 cm to 17.5 cm

All slabs are placed on a gravel substrate with a dielectric constant lower than measured in concrete (Table 2), so wave propagation through the concrete-gravel substrate media is resulted in a change in the polarization of the EM wave.
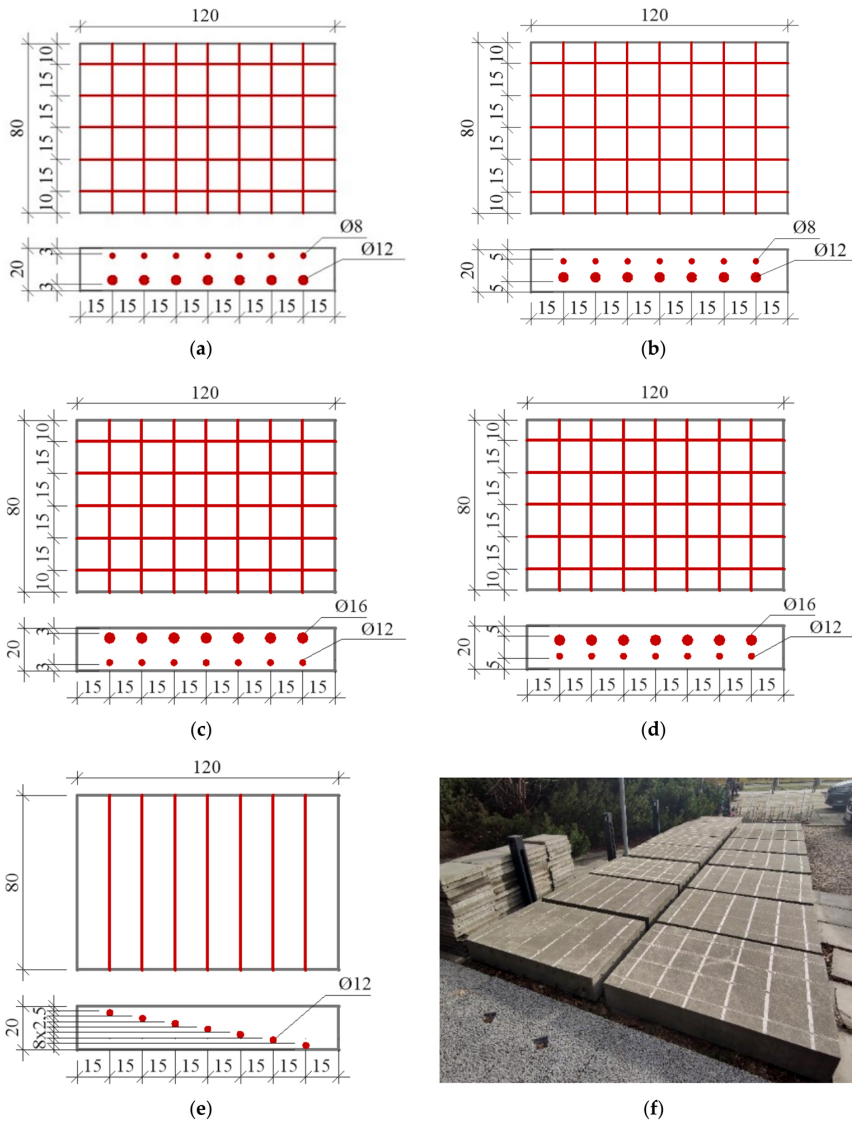
Fig. 3. Diagrams of concrete slabs with controlled discontinuities: slabs 1–5 used for testing: a) slab 1, b) slab 2, c) slab 3, d) slab 4, e) slab 5, f) including photo presenting test field; (photo: A. Lejzerowicz)

For the tests carried out on the testing site, only Slabs 1–5 containing rebars were used (Fig. 3), which could later be used to create a 3D model – visualization of the interior of the concrete slab using a point cloud. The research was conducted according to the drawn grid and on each slab 10 GPR profiles were collected in two directions perpendicular to each other: 4 profiles along the longer edge of the slab and 6 profiles along the shorter edge (Fig. 4). In the experiment only those along the longer edge were used because they were perpendicular to the rebars inside slabs.

Table 2. Dielectric constants of selected media based on [13, 31–33]

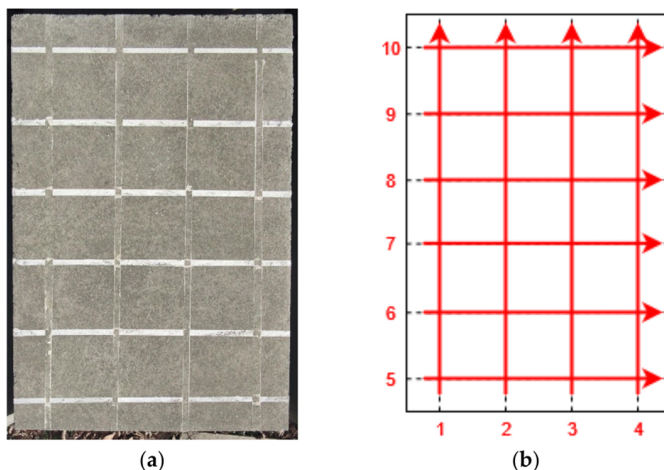| Medium	Dielectric constant [–]			
	[31]	[13]	[33]	[32]
air	1	1	1	1
water	81	81	81	81
sand	4–6	4–10 (dry) 10–30 (wet)	3–5 (dry) 20–30 (wet)	–
concrete	8–10	4–10 (dry) 10–20 (wet)	3–9	8 (old one) 10–20 (new one)
asphalt	4–8	2–4 (dry) 6–12 (wet)	2.5–3.5	4.5–6
gravel subgrade	4–7	–	–	8–15

Fig. 4. Photo of a single slab: a) with a scheme of GPR measurements, b) carried out on all five concrete slabs (photo: A. Lejzerowicz)

To collect lidar data a Leica RTC360 terrestrial laser scanner was used. The scanning range is from 0.5 up to 130 m, scanning rate is up to 2 million points/s. Angular resolution of the scanner is 18″, distance measurement accuracy is 1 mm + 10 ppm. Scanner is equipped with visual inertial system (VIS) for tracking in real time the path of the scanner's movement relative to the previous position. There are three scanning resolution settings to choose (3/6/12 mm by 10 m distance). Six scans were collected, at the highest possible scanning density setting (3 mm from 10 m distance) and with automatic point cloud coloring enabled. For georeferencing the scans, four targets were used, which were previously measured with a total station in the national reference system. Finally bundle adjustment error was at the level ±0.002 m.

3.2. Collecting and processing the GPR data

Three GPR antennas from different manufacturers and with various frequencies were used to collect GPR data: Antenna no. 1 with a frequency of 1600 MHz; Antenna no. 2 with a modulated frequency range of 200–4000 MHz, and Antenna no. 3 with a frequency of 1500 MHz. The parameters of the antennas are summarized in Table 3.

Table 3. Parameters of individual antennas used in the experiment

Parameter		Antenna no. 1	Antenna no. 2	Antenna no. 3
Frequency [MHz]		1600	200-4000	1500
Sampling	Horizontal [traces/m]	283	101	54
	Vertical [samples/scan]	512	409	500
Depth range [m]		0.8	0.5	0.8

The profiles were collected in the measurement grid shown in Fig. 5, and with each antenna, the tracing was performed in the same pattern. Figure 6 shows exemplary radargrams from Slab no. 1 collected with individual GPR antennas. The collected profiles were later processed in dedicated software for each antenna manufacturer. Basic processing of the collected data (background removal, gain control, zero-level determination) was performed. For all GPR profiles, the same propagation speed of the electromagnetic wave (10 cm/ns) was also established in the surveyed concrete slabs. All GPR profiles were then exported to .txt files for further processing in the developed script.
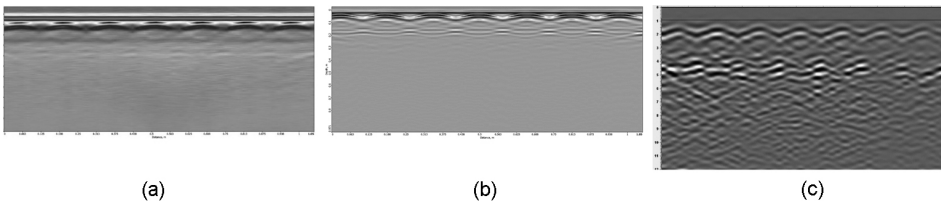

Fig. 5. Sample radargrams from Slab no. 1 for each of the used GPR antennas: a) Antenna no. 1: 1600 MHz, b) Antenna no. 2: modulated frequency range 200–4000 MHz, c) Antenna no. 3: 1500 MHz

The locations of the beginnings and ends of the profiles were measured on an oriented point cloud to maintain data consistency. Because of the differences in data recording formats by the different antennas, each antenna had a slightly different workflow, as summarized in the diagram in Fig. 6. The processing flow for individual GPR antennas is described below:

– Antenna no 1: the data from GPR were provided in .txt format in the form of amplitudes stored in a structured manner. For simpler data processing, this format was converted to a Antenna no. 3 standard format, and then the data processing workflow was the same as for the Antenna no. 3.

– Antenna no. 2: on the processed GPR data in dedicated software, files in NMEA format containing the beginnings and ends of each profile were loaded. Based on interpolation within the software, the coordinates of all intermediate traces were determined. The profiles were then exported to a text-based point cloud format. Lastly, the angular coordinates were changed from the WGS84 system to the TLS point cloud system. This was done using a Python script and the pyproj library.

– Antenna no. 3: the processed and exported GPR data for each profile consisted of two files: .dat and .gps. The .dat file contains the data in the form of path number, sample number, and amplitude value, as well as metadata, among other measurements of window depth and wave speed. The .gps file normally contains position information, but in our case, it was empty because we did not provide a real-time position to the antenna. To assign references using a Python script, valid .gps files were generated based on the known start and end points of the profile and the number of traces. The data prepared in this way was processed by the Python script, which transformed the data into point clouds in text format in the same reference system as the TLS point cloud.
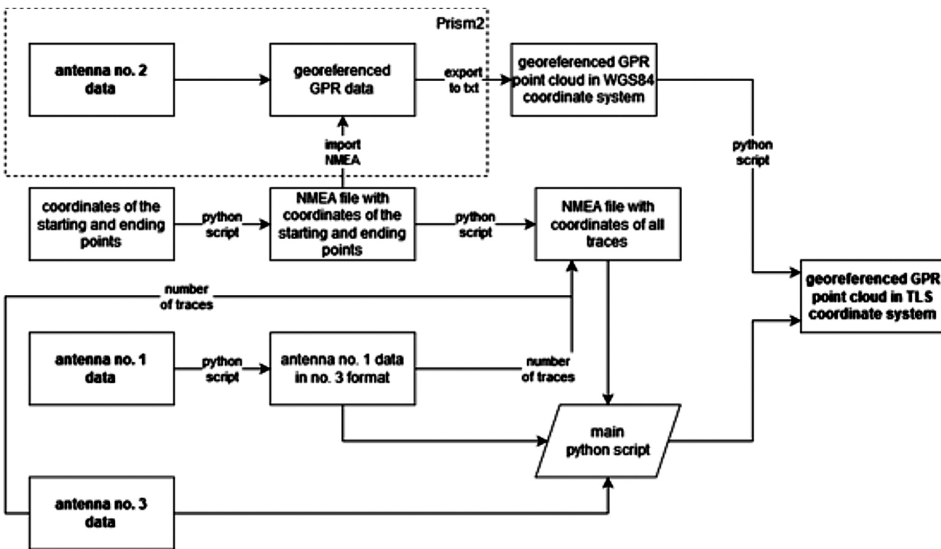

Fig. 6. Diagram presenting the processing workflow for different GPR antennas

Then, in CloudCompare software (version 2.10.2), 3D models of the rebars and slab outlines were drawn (Fig. 7) based on the project data. Based on the location of the corner points, the models were fitted using a 3D transformation and the top 4 corners of each slab. For each slab, the fit-in error was less than 2 mm. As a result, the reference models were transferred to the TLS reference system.
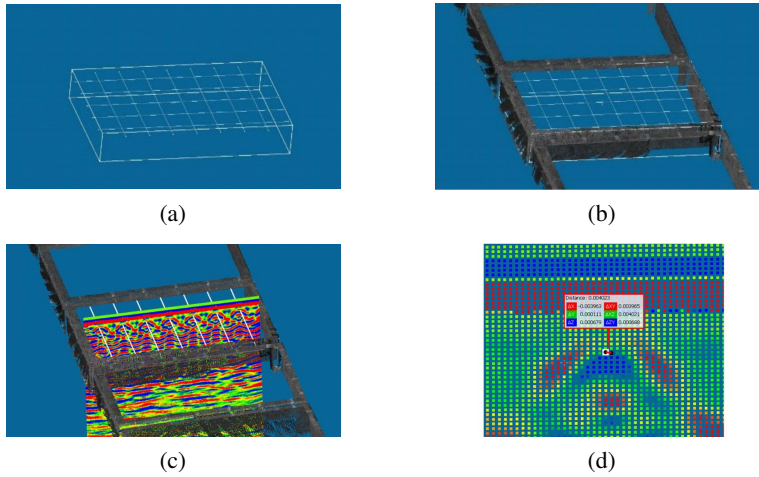
(a)

(b)

(c)

(d)

Fig. 7. Workflow steps in Cloud Compare: a) wireframe 3D model based dimensional sketch, b) transformation to lidar TLS data, c) visualization of GPR profile converted to 3D points in reference slab reference frame and, d) measurements showing differences between visible peak and reference location

4. Results

GPR measurements made on the five test concrete slabs taken with the three GPR antennas are presented in Fig. 8, where one exemplary GPR profile for each slab was shown. The same radargram was selected for each GPR antenna used during the tests. These are measurements perpendicular to the rebars, made along the longer edge of the slab. The results show the GPR profiles after processing in the program/script as described in Fig. 6. In each radargram, a white dot marks the location of individual reinforcing bars in each slab.

After indicating the location of the hyperbola vertex on each GPR image (Fig. 8), radargrams were integrated with the image obtained from TLS, creating 3D models showing the course of individual reinforcement bars within each slab (Fig. 9).

Table 4 shows the root mean square (RMS) error calculated for each slab, including standard deviations (STD) of observations. A slightly larger average error and a larger divergence of values were observed for the Antenna no. 1 and 3 than for the Antenna no. 2.

Table 4. The results of analysis for horizontal and vertical error for three antennas based on all observations for all five slabs

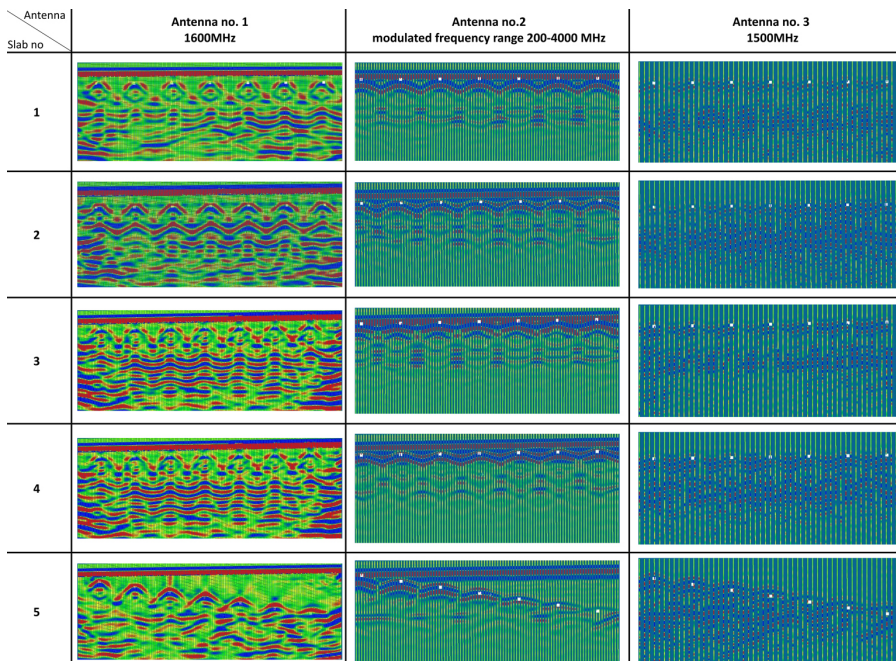| All slabs	XY			Z		
	Antenna no. 1	Antenna no. 2	Antenna no. 3	Antenna no. 1	Antenna no. 2	Antenna no. 3
RMS [m]	0.006	0.003	0.006	0.004	0.003	0.004
STD [m]	0.004	0.002	0.003	0.004	0.003	0.004

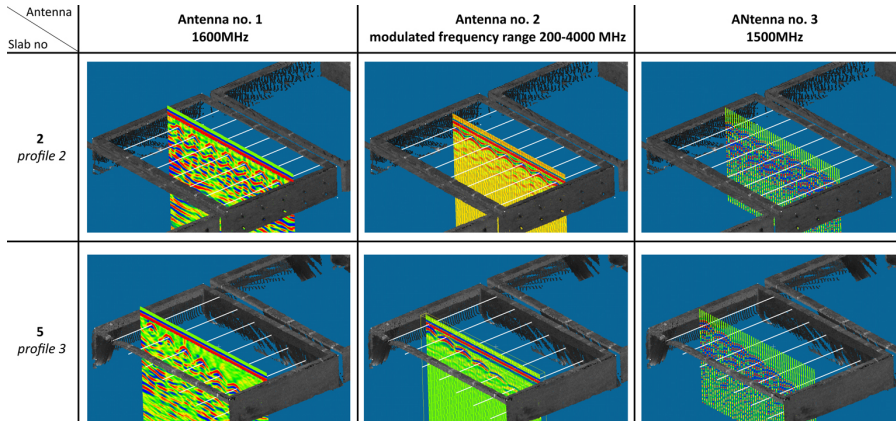Fig. 8. Cross sections for GPR measurements on concrete slabs no. 1–5

Fig. 9. GPR measurements (cross-sections) on slab 2 profile no 2 and slab 5 profile no 3 overlaying TLS reference point cloud

With the huge number of observations (140 horizontal observations and 140 vertical observations for each slab), it is difficult to analyze the specific result. It is difficult to draw conclusions when the values differ so slightly: the discrepancies between them are too small to be analyzed based on general statistics, encouraging deeper examination. In addition, one of the slabs (number 5) had bars at different depths (Fig. 3); therefore, in the next table (Table 5), it was decided to exclude this plate for the first, more detailed calculations.

Slab no. 2, profiles no. 1-4

Antenna no. 1

	1		2		3		4	
XY	Z	XY	Z	XY	Z	XY	Z
0,011	-0,004	0,003	-0,001	0,008	-0,002	0,007	-0,002
0,003	-0,001	0,003	0,002	0,001	-0,001	0,003	-0,005
0,002	0,002	0,001	0,002	0,005	0,002	0,003	-0,002
0,003	0,002	0,003	-0,001	0,002	0,002	0,002	-0,002
0,003	-0,001	0,001	-0,001	0,003	0,002	0,002	0,001
0,008	0,002	0,001	-0,001	0,001	0,002	0,002	-0,002
0,008	0,002	0,003	-0,001	0,005	0,002	0,002	-0,002

Antenna no. 2

	1		2		3		4	
XY	Z	XY	Z	XY	Z	XY	Z
0,011	-0,003	0,001	-0,001	0,010	-0,005	0,001	-0,005
0,007	-0,001	0,001	0,002	0,002	-0,002	0,002	-0,002
0,004	-0,001	0,001	0,002	0,003	0,000	0,004	-0,001
0,002	0,002	0,001	-0,001	0,000	-0,001	0,005	0,001
0,002	-0,001	0,001	-0,001	0,002	0,002	0,003	0,002
0,005	-0,001	0,001	-0,001	0,002	0,003	0,002	0,003
0,001	-0,001	0,001	-0,001	0,001	-0,003	0,000	-0,003

Antenna no. 3

	1		2		3		4	
XY	Z	XY	Z	XY	Z	XY	Z
0,003	-0,005	0,003	-0,001	0,002	-0,003	0,003	-0,002
0,008	-0,002	0,011	-0,004	0,005	0,000	0,009	-0,003
0,005	-0,001	0,006	-0,001	0,008	0,001	0,005	0,000
0,001	-0,002	0,000	-0,003	0,009	-0,001	0,001	-0,002
0,006	-0,002	0,006	-0,003	0,006	0,000	0,006	0,001
0,008	-0,002	0,008	-0,003	0,004	-0,001	0,008	0,000
0,002	-0,001	0,002	-0,003	0,001	0,001	0,002	0,000

Slab no. 5, profiles no. 1-4

Antenna no. 1

	1		2		3		4	
XY	Z	XY	Z	XY	Z	XY	Z
0,003	0,002	0,004	-0,001	0,001	-0,002	0,002	0,002
0,001	-0,001	0,001	-0,002	0,001	-0,005	0,002	-0,004
0,001	-0,004	0,007	-0,005	0,009	-0,005	0,003	-0,007
0,002	-0,005	0,007	-0,005	0,010	-0,008	0,003	-0,011
0,001	-0,005	0,010	-0,005	0,014	-0,009	0,006	-0,011
0,001	-0,005	0,009	-0,006	0,014	-0,009	0,005	-0,011
0,002	-0,006	0,005	-0,006	0,007	-0,009	0,005	-0,015

Antenna no. 2

	1		2		3		4	
XY	Z	XY	Z	XY	Z	XY	Z
0,000	0,007	0,001	0,004	0,000	0,005	0,001	0,004
0,003	-0,001	0,001	0,001	0,001	-0,003	0,001	-0,001
0,005	-0,004	0,002	-0,004	0,001	-0,006	0,002	0,004
0,002	0,003	0,003	0,002	0,001	0,003	0,003	-0,003
0,000	0,000	0,004	-0,001	0,002	0,000	0,004	-0,004
0,004	-0,001	0,005	0,001	0,002	-0,001	0,004	-0,002
0,007	-0,004	0,007	-0,007	0,002	-0,009	0,003	-0,005

Antenna no. 3

	1		2		3		4	
XY	Z	XY	Z	XY	Z	XY	Z
0,001	0,004	0,002	0,003	0,002	0,005	0,001	0,006
0,004	0,003	0,004	-0,001	0,004	-0,001	0,004	-0,002
0,006	-0,007	0,006	-0,005	0,007	-0,005	0,006	-0,007
0,009	-0,009	0,008	-0,010	0,009	-0,009	0,009	-0,010
0,008	-0,013	0,008	-0,010	0,008	-0,012	0,008	-0,010
0,005	-0,012	0,005	-0,012	0,005	-0,013	0,005	-0,012
0,002	-0,015	0,003	-0,007	0,003	-0,012	0,002	-0,013

Fig. 10. Horizontal and vertical differences between measured and reference location for two example slabs (Slab no. 2 and 5); values coloured with conditional formatting (red values – positive, blue values – negative)

In Table 5, only slabs with rebars at the same depth were analyzed, which, however, did not change the results of horizontal accuracy, which was twice higher than the height error resulting from difficulties in the interpretation (determination) of the vertex of the hyperbola. Moreover, in the horizontal accuracy (RMS), Antenna no. 1 and 3 have twice worse accuracy, which is caused by the sampling frequency for the Antenna no. 3 (Table 3) and the use of modulated frequency for the Antenna no. 2, which is the best here.

Table 5. The results of analysis for horizontal and vertical error for all three antennas limited to all observations for comparable slabs no. 1–4

Slabs 1–4	XY			Z		
	Antenna no. 1	Antenna no. 2	Antenna no. 3	Antenna no. 1	Antenna no. 2	Antenna no. 3
RMS [m]	0.006	0.003	0.006	0.002	0.003	0.003
STD [m]	0.004	0.002	0.003	0.002	0.003	0.003

In the next step, individual slabs were analyzed in terms of the replicability of the measurement between successive GPR cross-sections, and the replicability on the same bars within the slabs, and focusing on Slab no. 5 containing bars at different depths.

In the further part of the verification, the replicability of measurements was tested. Assuming that the rebars are at the same depth (known technical documentation, Fig. 3), the replicability of measurements on individual radargrams in each of the slabs was analysed. These results showed 2–3 times worse horizontal accuracy results for fixed frequency antennas. The results were not affected by the internal structure of the slab, in which the two rows of rebars were at different depths to each other (Table 6).

Table 6. The results of analysis for horizontal and vertical error for all three antennas limited to all observations for comparable slabs no. 1–4

Accuracy	XY [m]				
Slab no. Antenna	Slab 1	Slab 2	Slab 3	Slab 4	Slab 5
Antenna no.1	0.006	0.004	0.005	0.008	0.006
Antenna no.2	0.003	0.004	0.002	0.003	0.003
Antenna no.3	0.006	0.006	0.006	0.006	0.006
Accuracy	Z [m]				
Slab no. Antenna	Slab 1	Slab 2	Slab 3	Slab 4	Slab 5
Antenna no.1	0.003	0.002	0.001	0.002	0.007
Antenna no.2	0.004	0.002	0.002	0.003	0.003
Antenna no.3	0.002	0.002	0.004	0.002	0.009

The change in the height of successive rebars also did not affect the results obtained on Slab no. 5. For vertical accuracy, comparable results can be seen for slabs no. 1–4, but for Slab no. 5, in which the rebars are already at a different height, the clear errors increased 3–4 times for antennas no. 1 and 3. For the Antenna no. 2, they remained at the same level.

For a more thorough verification of this effect, the analysis was repeated by computing the accuracy statistics not for profiles, but for individual rebars (Table 7). In these two examples, slabs you can see that slab number 2 has an example of a constant error of a few millimetres. In the case of some measurements, higher values were observed on the first (edge) rebars, which can be interpreted as the influence of the edges on the reflectivity of the EM wave. Slightly worse results were observed for single frequency antennas.

For Slab no. 5 (Table 7), where each successive rebar was placed 2.5 cm deeper, the decrease in both horizontal and vertical accuracy is visible. In the case of one of the antennas, its construction prevented the measurement at the slab border, hence there are no measurements on one rebar located at its edge. With the increase in depth from 2.5 to 17.5 cm, the accuracy decreased 2–3 times for the antennas no. 1 and 3, there were no significant changes for the frequency modulated antenna (no. 2).

In further analysis, it was decided to check what this trend looks like and whether it can be confirmed by linear regression. However, when statistically analysing the trend lines for vertical and horizontal accuracy, we can see the visible effect of high standard deviations of measurements (Fig. 11a). Due to these deviations, the determination coefficient referring to the fit of the trend line to the observations, does not assume high values for horizontal accuracy, so we cannot talk about a trend - rather, this accuracy is like random errors proved observed accuracy. Analyzing the graph of vertical errors (Fig. 11b) for a slab that had rebars at an increasing depth, we can notice a visible upward trend despite the dispersion

Table 7. The accuracy statistics for individual rebars on successive radargrams for slabs no. 2 and 5

Accuracy	XY [m]			Z [m]		
Slab 2	Antenna no. 1	Antenna no. 2	Antenna no. 3	Antenna no. 1	Antenna no. 2	Antenna no. 3
Rebar 1	0.008	0.007	0.003	0.003	0.004	0.003
Rebar 2	0.003	0.004	0.009	0.003	0.002	0.003
Rebar 3	0.003	0.003	0.006	0.002	0.001	0.001
Rebar 4	0.003	0.003	0.005	0.002	0.001	0.002
Rebar 5	0.002	0.002	0.006	0.001	0.002	0.002
Rebar 6	0.004	0.003	0.007	0.002	0.002	0.002
Rebar 7	0.005	0.001	0.002	0.002	0.002	0.002
Slab 5	Antenna no. 1	Antenna no. 2	Antenna no. 3	Antenna no. 1	Antenna no. 2	Antenna no. 3
Rebar 1	0.003	0.001	0.002	0.002	0.005	0.005
Rebar 2	0.001	0.002	0.004	0.003	0.002	0.002
Rebar 3	0.006	0.003	0.006	0.005	0.005	0.006
Rebar 4	0.006	0.002	0.009	0.008	0.003	0.010
Rebar 5	0.009	0.003	0.008	0.008	0.002	0.011
Rebar 6	0.009	0.004	0.005	0.008	0.001	0.012
Rebar 7	0.005	0.005	0.003	0.010	0.007	0.012

of values. The greater the depth, the greater the error. This relationship for antennas no. 1 and 3 was confirmed by R2 over 0.8. In both cases, however, this trend was a decrease in accuracy of 0.05–0.07 cm with every 1 cm in depth.
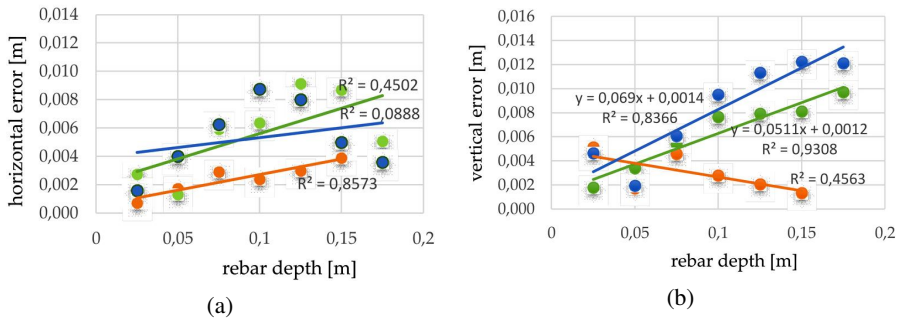
Fig. 11. The relation of: a) horizontal and, b) vertical mean square error versus the depth of the rebar in the Slab no. 5 with the trend calculated with linear regression confirmed by determination coefficient R2 (green – Antenna no. 1, orange – Antenna no. 2, blue – Antenna no. 3)

5. Discussion and conclusion

The conducted research shows an example of the use of GPR data and TLS in an example where GPR data is not used for interpretation itself but for precise determination of the horizontal and vertical position of objects located in inaccessible space.

The experiment used reference data in the form of concrete slabs in which the position of the rebars was known with great accuracy. TLS point clouds, which were oriented with millimeter accuracy, were used as data for GPR orientation in the reference system.

In other publications, comparable research results to those presented in this article can be found. However, they either pertained to one sensor exclusively, focused on object detection algorithms, or measured objects located at a constant depth level. In [7], an antenna of frequency 800 MHz was used, and a cylindrical PVC pipe with a wall thickness of 0.3 cm and inner diameter of 10 cm buried in the sand was automatically detected. The mean absolute error (MAE) and root mean squared (RMS) error of the location estimation were 0.005 and 0.007 m and for the depth estimation: 0.019 and 0.024 m for MAE and RMSE, respectively. In [34], antennas of three different frequencies were used (300, 600, and 900 MHz) and an automatic method of cracks, water-damage pits, and uneven settlements detection was presented. In these tests, the accuracy of the algorithm was 0.002 m.

The article analyzes the results obtained using three different GPR antennas, which were characterized by different sampling parameters, but also the used frequency of emitted EM waves with which the data was acquired. In the experiment, in numerous measurements, the vertical and horizontal accuracy of the measurement for each of the antennas was estimated, which was significantly below 1 cm in all antennas. In addition, all antennas have two times better vertical than horizontal accuracy, which is caused by the difficulty of interpreting and detecting the hyperbola vertex on radargrams and the fact that vertical sampling is higher than the horizontal one. It was noticed that single frequency antennas have about two times lower accuracy than the antenna with modulated frequency, which was proven in the example of Slab no. 5, characterized by the presence of reinforcing bars placed in the concrete at variable depths. It was also concluded that the frequency modulated antenna copes much better with the accuracy of vertical measurements. Those conclusions are useful in detailed surveying measurements using non-destructive remote sensing sensors like GPR antenna.

Acknowledgements

References

[1] N. Iftimie, A. Savin, R. Steigmann, and G.S. Dobrescu, "Underground Pipeline Identification into a Non-Destructive Case Study Based on Ground-Penetrating Radar Imaging", *Remote Sensing (Basel)*, vol. 13, no. 17, 2021, doi: 10.3390/rs13173494.

[2] W. Zhao, L. Yuan, E. Forte, G. Lu, G. Tian, and M. Pipan, "Multi-Frequency GPR Data Fusion with Genetic Algorithms for Archaeological Prospection", *Remote Sensing (Basel)*, vol. 13, no. 14, 2021, doi: 10.3390/rs13142804.

[3] M. Solla, V. Pérez-Gracia, and S. Fontul, "A Review of GPR Application on Transport Infrastructures: Troubleshooting and Best Practices", *Remote Sensing (Basel)*, vol. 13, no. 4, 2021, doi: 10.3390/rs13040672.

[4] A. Joshaghani and M. Shokrabadi, "Ground penetrating radar (GPR) applications in concrete pavements", *International Journal of Pavement Engineering*, vol. 23, no. 13, pp. 4504–4531, 2022, doi: 10.1080/10298436.2021.1954182.

[5] S. Cafiso, A. Di Graziano, D. Goulias, M. Mangiameli, and G. Mussumeci, "Implementation of GPR and TLS Data for the Assessment of the Bridge Slab Geometry and Reinforcement", *Archives of Civil Engineering*, vol. 66, no. 1, pp. 297–308, 2020, doi: 10.24425/ace.2020.131789.

[6] J. Li, T. Guo, H. Leung, H. Xu, L. Liu, B. Wang, and Y. Liu, "Locating Underground Pipe Using Wideband Chaotic Ground Penetrating Radar", *Sensors*, vol. 19, no. 13, 2019, doi: 10.3390/s19132913.

[7] S. Jazayeri, A. Saghafi, S. Esmaeili, and C. P. Tsokos, "Automatic object detection using dynamic time warping on ground penetrating radar signals", *Expert Systems with Applications,* vol. 122, pp. 102–107, 2019, doi: 10.1016/j.eswa.2018.12.057.

[8] I. Puente, M. Solla, S. Lagüela, and J. Sanjurjo-Pinto, "Reconstructing the Roman Site 'Aquis Querquennis' (Bande, Spain) from GPR, T-LiDAR and IRT Data Fusion", *Remote Sensing (Basel)*, vol. 10, no. 3, 2018, doi: 10.3390/rs10030379.

[9] S. Ogunniyi, D. Withey, S. Marais, and G. Crafford, "LiDAR-based 3D Mapping and Localisation System for Ground Penetrating Radar", in *2020 International SAUPEC/RobMech/PRASA Conference*. IEEE, 2020, pp. 1–6, doi: 10.1109/SAUPEC/RobMech/PRASA48453.2020.9041134.

[10] M. Grasmueck and D. A. Viggiano, "Integration of Ground-Penetrating Radar and Laser Position Sensors for Real-Time 3-D Data Fusion", *IEEE Transactions on Geoscience and Remote Sensing*, vol. 45, pp. 130–137, 2007.

[11] M.S. Sudakova, M. Sadurtdinov, A. Tsarev, A. Skvortsov, and G. Malkova, "Ground-Penetrating Radar for Studies of Peatlands in Permafrost", *Russian Geology and Geophysics*, vol. 60, no. 7, pp. 793–800, 2019.

[12] T. Yamaguchi, T. Mizutani, M. Tarumi, and D. Su, "Sensitive Damage Detection of Reinforced Concrete Bridge Slab by 'Time-Variant Deconvolution' of SHF-Band Radar Signal", *IEEE Transactions on Geoscience and Remote Sensing*, vol. 57, no. 3, pp. 1478–1488, 2019, doi: 10.1109/TGRS.2018.2866991.

[13] D.J. Daniels, *Ground Penetrating Radar*. Institution of Engineering and Technology, 2004, doi: 10.1049/PBRA015E.

[14] N.J. Cassidy, R. Eddies, and S. Dods, "Void detection beneath reinforced concrete sections: The practical application of ground-penetrating radar and ultrasonic techniques", *Journal of Applied Geophysics*, vol. 74, no. 4, pp. 263–276, 2011, doi: 10.1016/j.jappgeo.2011.06.003.

[15] M. Ramya, K. Balasubramaniam, and M. Shunmugam, "On a reliable assessment of the location and size of rebar in concrete structures from radargrams of ground-penetrating radar", *Insight - Non-Destructive Testing and Condition Monitoring*, vol. 58, no. 5, pp. 264–270, 2016, doi: 10.1784/insi.2016.58.5.264.

[16] K. Dinh, N. Gucunski, and T. Duong, "Migration-based automated rebar picking for condition assessment of concrete bridge decks with ground penetrating radar", *NDT & E International*, vol. 98, pp. 45–54, 2018, doi: 10.1016/j.ndteint.2018.04.009.

[17] A. Benedetto and F. Benedetto, "Application Field–Specific Synthesizing of Sensing Technology", in *Comprehensive Materials Processing*. Elsevier, 2014, pp. 393–425, doi: 10.1016/B978-0-08-096532-1.01315-7.

[18] Z. Xiang, G. Ou, and A. Rashidi,37 "An Innovative Approach to Determine Rebar Depth and Size by Comparing GPR Data with a Theoretical Database", in *Construction Research Congress 2020: Computer Applications*. ASCE, 2020, pp. 86–95, doi: 10.1061/9780784482865.010.

[19] K. Agred, G. Klysz, and J. Balayssac, "Location of reinforcement and moisture assessment in reinforced concrete with a double receiver GPR antenna", *Construction and Building Materials*, vol. 188, pp. 1119–1127, 2018, doi: 10.1016/j.conbuildmat.2018.08.190.

[20] M.R. Shaw, S. G. Millard, T.C.K. Molyneaux, M.J. Taylor, and J.H. Bungey, "Location of steel reinforcement in concrete using ground penetrating radar and neural networks", *NDT & E International*, vol. 38, no. 3, pp. 203–212, 2005, doi: 10.1016/j.ndteint.2004.06.011.

[21] Z. Xiang, A. Rashidi, and G. (Gaby) Ou, "An Improved Convolutional Neural Network System for Automatically Detecting Rebar in GPR Data", in *Computing in Civil Engineering 2019: Data, Sensing, and Analytics*. ASCE, 2019, pp. 422–429, doi: 10.1061/9780784482438.054.37

[22] P. Wiwatrojanagul, R. Sahamitmongkol, S. Tangtermsirikul, and N. Khamsemanan, "A new method to determine locations of rebars and estimate cover thickness of RC structures using GPR data", *Construction and Building Materials*, vol. 140, pp. 257–273, 2017, doi: 10.1016/j.conbuildmat.2017.02.126.

[23] H. Rathod, S. Debeck, R. Gupta, and B. Chow, "Applicability of GPR and a rebar detector to obtain rebar information of existing concrete structures", *Case Studies in Construction Materials*, vol. 11, art. no. e00240, 2019, doi: 10.1016/j.cscm.2019.e00240.

[24] Z. Xiang, A. Rashidi, and G. Ou, "States of Practice and Research on Applying GPR Technology for Labeling and Scanning Constructed Facilities", *Journal of Performance of Constructed Facilities*, vol. 33, no. 5, 2019, doi: 10.1061/(ASCE)CF.1943-5509.0001313.

[25] F. Zhou, Z. Chen, H. Liu, J. Cui, B.F. Spencer, and G. Fang, "Simultaneous Estimation of Rebar Diameter and Cover Thickness by a GPR-EMI Dual Sensor", *Sensors*, vol. 18, no. 9, 2018, doi: 10.3390/s18092969. 37

[26] W. Mukupa, G.W. Roberts, C.M. Hancock, and K. Al-Manasir, "A review of the use of terrestrial laser scanning application for change detection and deformation monitoring of structures", *Survey Review*, vol. 49, no. 353, pp. 99–116, 2017, doi: 10.1080/00396265.2015.1133039.

[27] H. Li, S. Qi, X. Yang, X. Li, and J. Zhou, "Geological Survey and Unstable Rock Block Movement Monitoring of a Post-Earthquake High Rock Slope Using Terrestrial Laser Scanning", *Rock Mechanics and Rock Engineering*, vol. 53, no. 10, pp. 4523–4537, 2020, doi: 10.1007/s00603-020-02178-0.

[28] N. Lercari, "Monitoring earthen archaeological heritage using multi-temporal terrestrial laser scanning and surface change detection", *Journal of Cultural Heritage*, vol. 39, pp. 152–165, 2019, doi: 10.1016/j.culher.2019.04.005.

[29] X. Liang, et al., "Terrestrial laser scanning in forest inventories", *ISPRS Journal of Photogrammetry and Remote Sensing*, vol. 115, pp. 63–77, 2016, doi: 10.1016/j.isprsjprs.2016.01.006.

[30] C. Wu, Y. Yuan, Y. Tang, and B. Tian, "Application of Terrestrial Laser Scanning (TLS) in the Architecture, Engineering and Construction (AEC) Industry", *Sensors*, vol. 22, no. 1, 2022, doi: 10.3390/s22010265.

[31] T. Saarenketo, "Electrical properties of road materials and subgrade soils and the use of Ground Penetrating Radar in traffic infrastructure surveys", PhD thesis, University of Oulu, Finland, 2006.

[32] X. Han, "Experimental Study on Dielectric Properties of Pavement Structure Layer Based on Radar Image", *Chemical Engineering Transactions*, vol. 66, pp. 883–888, 2018, doi: 10.3303/CET1866148.

[33] J. Karczewski, Ł. Ortyl, and M. Pasternak, *Zarys Metody Georadarowej*. Kraków, Poland: Wydawnictwa AGH, 2011.

[34] Z. Tong, D. Yuan, J. Gao, Y. Wei, and H. Dou, "Pavement-distress detection using ground-penetrating radar and network in networks," *Construction and Building Materials*, vol. 233, art. no. 117352, 2020, doi: 10.1016/j.conbuildmat.2019.117352.

Analiza dokładności określania lokalizacji obiektów podziemnych za pomocą georadaru z wykorzystaniem danych lidarowych

Słowa kluczowe: GPR, lidar, płyty betonowe, TLS, wizualizacja, zbrojenie

Streszczenie:

Georadar jest jedną z najbardziej użytecznych nieinwazyjnych technik lokalizowania obiektów podziemnych. Postęp w tej technologii w ostatniej dekadzie ułatwił rozwój nowych sensorów. W artykule przedstawiono ocenę dokładności lokalizacji prętów zbrojeniowych znajdujących się w obrębie

badanego obiektu z wykorzystaniem różnych anten. Aby osiągnąć założone cele, wykonano pomiary 5 płyt betonowych, zbrojonych prętami stalowymi o różnych średnicach i znajdujących się na różnych głębokościach. Eksperyment obejmował wykorzystanie trzech anten o różnej częstotliwości do oceny rozmiaru, charakterystyki i różnic wyodrębnionych danych. W metodyce eksperymentu wykorzystano dodatkowo dane lidarowe z naziemnego skanowania laserowego (TLS), aby zapewnić precyzyjne pomiary powierzchni, a tym samym zewnętrzną orientację przestrzenną pozyskanych danych. Eksperyment pozwolił na wyznaczenie dokładności pionowej i poziomej dla trzech wykorzystanych anten oraz ocenę rosnącej wartości błędów wraz z większą głębokością mierzonych elementów, co jest istotne dla predykcji dokładności pomiarów.